Journal of Animal & Plant Sciences, 36(1): 2026, Page: 16-26
ISSN (print): 1018-7081; ISSN (online): 2309-8694
https://doi.org/10.36899/JAPS.2026.1.0002

MECHANISM OF PROPOFOL ON CARDIAC FUNCTION IN RATS WITH AUTOIMMUNE MYOCARDITIS VIA REGULATION OF HMGB1-RAGE SIGNALING

J. D. Lv*, L.L. Zhang and S. J. Liu

Department of Anesthesiology, Jiashan County First People's Hospital, Jiashan, 314100, Zhejiang, China.
*Corresponding author's Email: lvjidonglv@126.com

ABSTRACT

The experimental autoimmune myocarditis (EAM) remains an urgent issue to be addressed. The high mobility group box-1 (HMGB1)-receptor for advanced glycation endproducts (RAGE) signaling acts imperatively in pathogenesis of myocarditis. The aim of this study was to evaluate the potential mechanism of various doses of propofol in enhancing the cardiac function of EAM rats and its role in regulating HMGB1-RAGE signal transduction. Fifty rats were randomly and equally assigned to Control, EAM, low-dose propofol (LDP), medium-dose propofol (MDP), and high-dose propofol (HDP) groups. Control group received phosphate-buffered saline (PBS) injection (1 mL, oral gavage). EAM, LDP, MDP, and HDP groups were induced with EAM via porcine myocardial protein injection. Following model establishment, LDP, MDP, and HDP were delivered consecutively at 25, 50, and 100 mg/kg, respectively. Echocardiography assessed cardiac function parameters, namely left ventricular end-systolic diameter (LVESD, mm), LV end-diastolic diameter (LVEDD, mm), LV fractional shortening (LVFS), LV ejection fraction (LVEF). The serum cytokine levels were measured. Myocardial tissue was harvested for histopathological examination by Hematoxylin-eosin staining and scoring. The expression of MMP-3, MMP-9, TIMP-1, IL-1β, and inducible nitric oxide synthase (iNOS) in myocardial tissue was determined. Western blotting assessed the protein level of HMGB1 and RAGE in myocardial tissue. Compared with the Control group, EAM group exhibited significantly increased values of LVESD and LVEDD, higher myocardial inflammation scores, and elevated TNF-α, IFN-γ, TGF-β1, IL-17, MMP-3, MMP-9, IL-1β, iNOS mRNA expression, and HMGB1 and RAGE protein expression ($P \leq 0.05$). In contrast, LVFS and LVEF values, IL-4 and IL-10 levels, and TIMP-1 mRNA expression were significantly decreased ($P \leq 0.05$). However, compared with EAM group, MDP and HDP groups showed significantly reduced LVESD and LVEDD values, myocardial inflammation scores, and reduced TNF-α, IFN-γ, TGF-β1, IL-17, MMP-3, MMP-9, IL-1β, iNOS mRNA expression, and HMGB1 and RAGE protein expression ($P \leq 0.05$), while LVFS and LVEF values, IL-4 and IL-10 levels, and TIMP-1 mRNA expression were significantly increased ($P \leq 0.05$). Propofol improves cardiac function in EAM rats by modulating the balance between pro-inflammatory (Th1, Th17) and anti-inflammatory (Th2, Treg) responses and suppressing myocardial inflammation, an effect that may involve inhibition of the HMGB1-RAGE signaling pathway.

Keywords: Experimental autoimmune myocarditis; propofol; cardiac function; HMGB1-RAGE signaling

Published first online December 15, 2025 Published final January 20, 2026

INTRODUCTION

Experimental autoimmune myocarditis (EAM) predominantly affects young adults, and immune dysfunction induced by viral infections is the primary pathogenic mechanism of EAM (Gajić *et al.,* 2021). EAM causes myocarditis-related death in young patients, with over 30% of affected individuals progressing to heart failure (Tschöpe *et al.,* 2021). Currently, no effective treatment exists for EAM, making the identification of therapeutic targets and effective drugs crucial. The cardiovascular system in rats closely resembles that of humans, and their immune system is well-developed, making them suitable for modeling the pathological process of human myocarditis. Rats have been widely utilized in research on myocarditis and other heart-related diseases, and in this work, EAM rat model was established to lay the groundwork for subsequent research.

Propofol is a widely utilized short-acting intravenous anesthetic, primarily acting by enhancing the inhibitory effects of γ-aminobutyric acid (GABA) to produce central nervous system depression, thus rapidly inducing and maintaining anesthesia (Burnett *et al.,* 2023). It has a fast onset, short duration of action, rapid recovery, and relatively mild suppression of the respiratory and circulatory systems, which has led to its extensive clinical application. In addition, propofol also exhibits anti-cancer and immune modulation properties. Studies noted that propofol can inhibit cell cycle-related

protein expression, blocking the G1 phase of tumor cells to suppress their proliferation (Sun *et al.,* 2024). Furthermore, propofol can induce tumor cell apoptosis by triggering mitochondrial and death receptor pathways (Chang *et al.,* 2022). In immune modulation, propofol regulates T cell activation and differentiation, suppressing Th1 cell activity while promoting Th2 cell activity to maintain immune balance (Yamamoto *et al.,* 2024). Upon stimulation, NF-κB is activated and translocates into the nucleus, initiating the transcription and expression of a series of inflammation-related genes, thereby triggering an inflammatory response. Propofol suppresses NF-κB activation through multiple mechanisms, including inhibiting the phosphorylation of upstream signaling molecules and reducing its nuclear translocation, ultimately leading to decreased release of inflammatory mediators and attenuation of inflammation (Wu *et al.,* 2020). Inflammatory responses and oxidative stress play key roles in myocardial injury. Zhang *et al*. found that propofol treatment of human umbilical vein endothelial cell-derived microvesicles could inhibit oxidative stress and apoptosis in cells (Zhang *et al.,* 2023). Huang *et al*. found that propofol could reduce the myocardial infarct area in diabetic myocardial infarction/reperfusion rats, as well as inhibit oxidative stress and myocardial cell apoptosis (Huang *et al.,* 2022). Another study also confirmed that propofol could reduce doxorubicin-induced myocardial cell apoptosis and mediate the PI3K/Akt signaling to exert myocardial protective effects (Zhang *et al.,* 2022). Xie *et al*. (2024) further demonstrated that propofol could reverse lipopolysaccharide-induced cardiac structural changes and dysfunction, primarily by inhibiting oxidative stress and apoptosis in myocardial cells, thus offering cardioprotection in septic conditions (Xie *et al.,* 2024). Briefly, besides its anesthetic properties, propofol also has anti-cancer, anti-inflammatory, and cardioprotective effects. Nevertheless, whether propofol can protect cardiac function in EAM still needs further investigation.

Propofol reduces the release of inflammatory cytokines and suppresses excessive immune system activation. It is thus hypothesized that propofol may modulate immune function through its anti-inflammatory properties by influencing immune cell activity and the secretion of cytokines. These immunomodulatory effects could ameliorate the inflammatory microenvironment in myocardial tissue, attenuate cellular damage and stress, and consequently indirectly inhibit the translocation of HMGB1 from the nucleus to the extracellular space, thereby reducing the activation of the HMGB1-RAGE signaling pathway. Based on this, the present work established an EAM rat model to analyze the effects of different doses of propofol to evaluate its effects on cardiac function, immune regulation, myocardial inflammatory response, and modulation of the HMGB1-RAGE signaling in EAM rats. We aimed to understand the pathogenesis of EAM and the potential mechanisms of propofol in cardiac function protection in EAM.

MATERIALS AND METHODS

Experimental animals: Fifty male Sprague Dawley rats (7 weeks old, 250-270 g; Beijing Huafu Kang Biotechnology Co., Ltd., China) were recruited and housed in laboratory at 23-26°C, 55-60% relative humidity, and a 12-h light/dark cycle. The study was approved by the Ethics Committee of Jiashan County First People's Hospital in accordance with all applicable guidelines and regulations.

Animal grouping: The rats were randomly assigned to Control, EAM, low-dose propofol (LDP), middle-dose propofol (MDP), and high-dose propofol (HDP) groups (n=10).

Control group: rats received 1 mL of PBS injection (Thermo Fisher Scientific, USA) into each of two inguinal regions.

EAM group: porcine myocardial protein (Sigma-Aldrich, USA) was first dissolved in 0.15 mol/L PBS, with concentration adjusted to 2 mg/mL. Porcine myocardial protein solution was emulsified with complete Freund's adjuvant (Sigma-Aldrich, USA) at a 1:1 ratio. The resulting emulsion was then injected into each of the two inguinal regions of the rats at 1 mL per site. After 7 consecutive days of injections, the success of model was evaluated by observing histopathological changes in myocardial tissue. Once the model was successfully established, rats were gavaged with 1 mL/100 g of saline for 28 d.

LDP group: the same model as EAM group was utilized. After successful modeling, rats were gavaged with 25 mg/kg propofol for 28 d.

MDP group: the same model as EAM group was utilized. After successful modeling, rats were gavaged with 50 mg/kg propofol for 28 d.

HDP group: the same model as EAM group was utilized. After successful modeling, rats were gavaged with 100 mg/kg propofol for 28 d.

Echocardiographic examination: Rats from each group were anesthetized with 30 mg/kg of 1% sodium pentobarbital (Sigma-Aldrich, USA) via intraperitoneal injection at 0, 1, 3, 7, 14, and 28 days after the start of gavage following successful modeling. Cardiac structural and functional changes were assessed using the IVIS Spectrum small animal ultrasound imaging system (Shanghai Ruifu Di Biomedical, China). The parameters evaluated included left ventricular end-systolic diameter (LVESD), LV end-diastolic diameter (LVEDD), LV fractional shortening (LVFS), and LV ejection fraction (LVEF). All echocardiographic examinations were performed and evaluated by experienced ultrasonographers, and the final values were obtained by

averaging the measurements from five consecutive cardiac cycles. The researchers responsible for image acquisition and data analysis were blinded to the experimental group assignments of the rats.

Hematoxylin-eosin staining for histopathological observation: After treatment and the final echocardiographic examination, rats were euthanized, and hearts were harvested following thoracotomy. Hearts were longitudinally sectioned along the coronal plane into two halves. One portion was stored at-80°C for future use, and the other was fixed in 4% paraformaldehyde (Sigma-Aldrich, USA) at 25°C. After 24 h of fixation in 4% paraformaldehyde, the heart tissue was dehydrated through successive immersions in 70%, 80%, 90%, 95%, 100%, and 100% ethanol for 1 h each. Tissue was treated with xylene I and xylene II (Xiongda Chemical Co., Ltd., China) for 30min each to clear the tissue. Following this, the tissue was infiltrated with paraffin at 60°C for 2 h using melted paraffin (Shanghai Ruichu Biotechnology Co., Ltd., China). Once solidified, tissue was sectioned into 4 μm slices via an S700 paraffin microtome (Shenzhen Ruiwode Co., Ltd., China). Sections were deparaffinized in xylene and rehydrated via ethanol. Tissue was stained with hematoxylin (Solarbio Technology Co., Ltd., China) for 5min, differentiated and blued via 1% hydrochloric acid ethanol and ammonia solution for 3 s, respectively. Then, eosin (Solarbio Technology Co., Ltd., China) was utilized for staining for 5min. Sections were mounted with neutral resin (Sigma-Aldrich, USA) following dehydration with ethanol in gradient and cleaning with xylene. The histopathological changes in myocardial tissue were visualized under a BX53M microscope (Olympus, Japan). Five random fields were selected for inflammation scoring based on inflammatory cell infiltration and necrosis area percentage, with scores assigned as follows: 0-25% as 1 point, 25-50% as 2, 50-75% as 3, and 75-100% as 4. The pathologists who performed the histological examination and scoring of myocardial tissue sections were blinded to the experimental group allocation of the samples to ensure objective evaluation of pathological features including myocardial inflammation severity, cellular infiltration, and tissue damage extent without investigator bias.

Enzyme-linked immunosorbent assay: After the final administration and echocardiographic examination, blood was collected from abdominal aorta, left at 25°C for 30min, centrifuged at 3000 rpm for 10min to separate the serum. Serum TNF-α, IFN-γ, IL-4, IL-10, TGF-β1, and IL-17 levels were measured with the ELISA kits (Shanghai Beyotime Biotechnology Co., Ltd., China). Each assay was performed in triplicate, and the average value was calculated.

Real-time quantitative PCR detection: A portion of the heart tissue stored at-80°C was utilized for RNA extraction via Trizol method (Sigma-Aldrich, USA). cDNA was synthesized via R transcription kit (Solarbio Technology Co., Ltd., China). Using cDNA as a template, real-time quantitative PCR was performed for myocarditis-related genes following the protocol provided with the Real-Time Quantitative PCR kit (Solarbio Technology Co., Ltd., China). The primer sequences for the quantitative PCR were matrix metalloproteinase-3 (MMP-3) F: 5'-ACATGGAGACTTTGTCCCTTTTG-3', R: 5'-TTGGCTGAGTGGTAGAGTCCC-3'; MMP-9 F: 5'-GGACCCGAAGCGGACATTG-3', R: 5'-CGTCGTCGAAATGGGCATCT-3'; Tissue inhibitor of metalloproteinase-1 (TIMP-1) F: 5'-CTTGGTTCCCTGGCGTACTC-3', R: 5'-ACCTGATCCGTCCACAAACAG-3'; IL-1β F: 5'-TGTGATGAAAGACGGCACAC-3', R: 5'-CTTCTTCTTTGGGTATTGTTTG-3'; iNOS F: 5'-ACCATGGAGCATCCCAAGT-3', R: 5'-CAGCGCATACCACTTCAGC-3'; β-actin F: 5'-TGGCTCTAACAGTCC GCCTAG -3', R: 5'-CGTTGACATCCGTAAAGACC -3'. PCR conditions were: 95°C for 3min (pre-denaturation), 95°C for 30s (denaturation), 60°C for 30s (annealing), 72°C for 30s (extension) for 30 cycles, 72°C for 5min (final extension). Target gene relative levels were computed utilizing $2^{-\Delta\Delta CT}$, with β-actin as internal reference. Each assay was implemented thrice to take average value.

Western blotting: Heart tissue stored at-80°C was homogenized in RIPA lysis buffer (Sigma-Aldrich, USA) to extract total protein. Bicinchoninic acid kit (Sigma-Aldrich, USA) determined protein concentration. After heat denaturation, the proteins were separated by SDS-PAGE, transferred onto a PVDF membrane, which was then blocked with 5% non-fat dry milk at 25°C for 1 h. After washing, membrane was incubated overnight at 4°C with primary antibodies against HMGB1, RAGE, and β-actin (Abcam, UK), each diluted 1:1000. After washing, the membrane was incubated with a secondary antibody, goat anti-mouse IgG (Abcam, UK), diluted 1:5000, at 25°C for 2 h. After washing, the membrane was subjected to enhanced chemiluminescence (Thermo Fisher Scientific, USA) detection, and the results were visualized using the WD-9413C Gel Imaging System (Beijing Liuyi Biotechnology Co., Ltd., China). β-actin was utilized as internal reference protein, and target protein relative levels were computed employing *Image J*. Each experiment was performed thrice to take average value.

Statistical analysis: Utilizing *SPSS 23*.0, data were denoted as mean ± standard deviation. One-way analysis of variance (One-way ANOVA) performed multiple-group comparisons. When homogeneity of variance was confirmed for quantitative data, the least significant

difference (LSD) method was subsequently employed for pairwise comparisons between groups. $P \leq 0.05$ was statistically significant.

RESULTS

Cardiac function: The differences in cardiac function parameters, including LVESD, LVEDD, LVFS, and LVEF, were evaluated across different groups of rats (Figure 1). The results indicated that negligible changes existed in the LVESD, LVEDD, LVFS, and LVEF parameters at different time points in Control group. In EAM group, LVESD and LVEDD significantly higher than those in Control group, while LVFS and LVEF were lower than Control group ($P \leq 0.05$). All measured parameters in LDP group showed improvement trends compared with the EAM group, but all were not considerable ($P > 0.05$). Nevertheless, in MDP and HDP groups, LVESD and LVEDD were significantly smaller, and LVFS and LVEF were notably larger compared with the LDP group ($P \leq 0.05$).

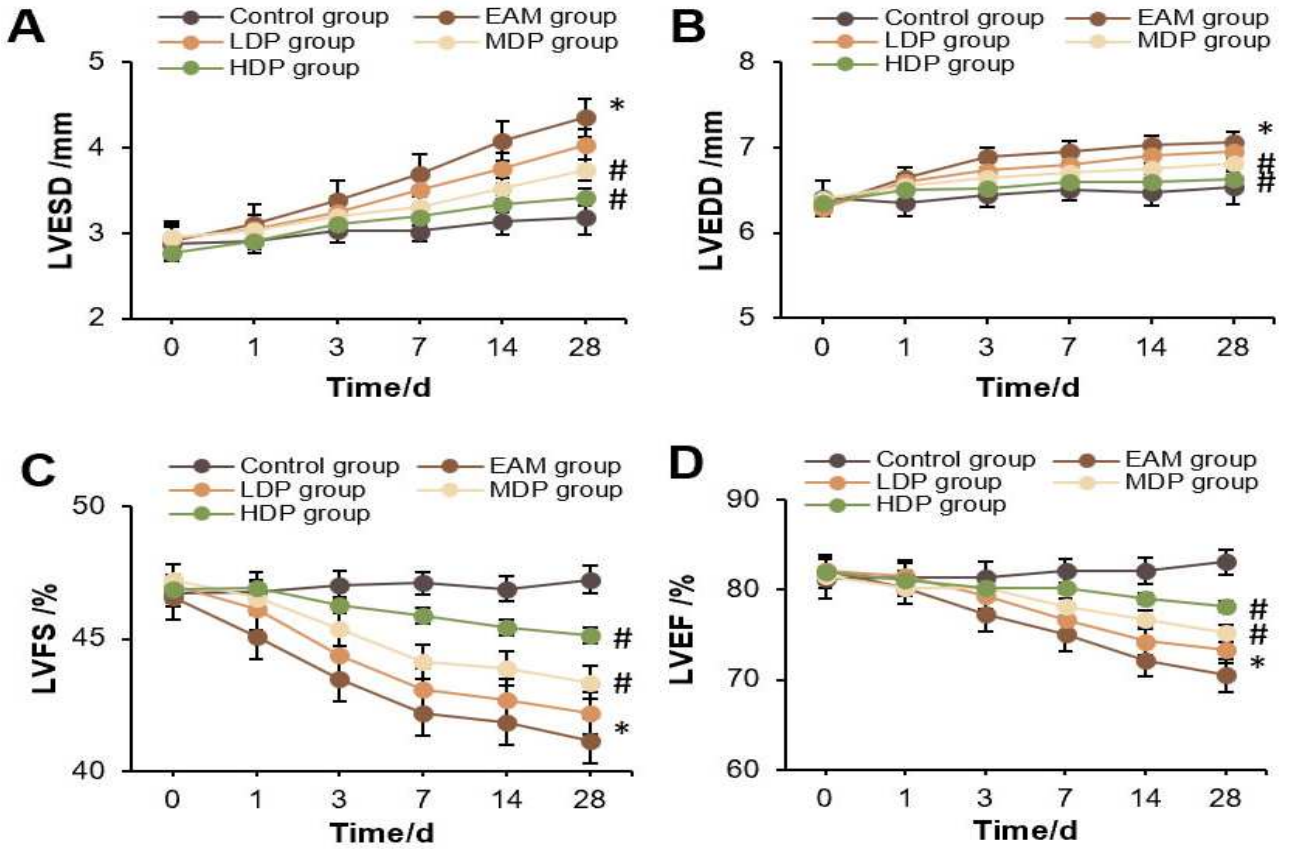

Figure 1. Contrast of cardiac function parameters among groups. (A) LVESD parameter; (B) LVEDD parameter; (C) LVFS parameter; (D) LVEF parameter. *$P \leq 0.05$ *vs.* Control group; #$P \leq 0.05$ *vs.* EAM group (in Figures 1-5).

Contrast of myocardial morphology among groups: The histopathological changes in myocardial tissue of rats were observed (Figure 2). The results revealed that the myocardial structure in Control group was intact, with regular arrangement of myocardial cells and fibers. In EAM group, the myocardial tissue exhibited disorganized cell arrangement, with observable pathological changes such as inflammatory cell infiltration, myocardial fiber rupture, and collagen fiber deposition. The myocardial structure in LDP group was somewhat improved when compared with the EAM group, although inflammatory cell infiltration, myocardial fiber rupture, and collagen fiber deposition were still present. The myocardial structure in MDP and HDP groups showed observable improvement, with HDP group's myocardial structure, as well as the arrangement of myocardial cells and fibers, being almost indistinguishable from Control group. The myocardial inflammation score in EAM group significantly surpassed that in Control group ($P \leq 0.05$). Negligible difference in myocardial inflammation score was observed between LDP and EAM groups ($P > 0.05$). However, the myocardial inflammation score in MDP and HDP groups was significantly lower to that in LDP group ($P \leq 0.05$).

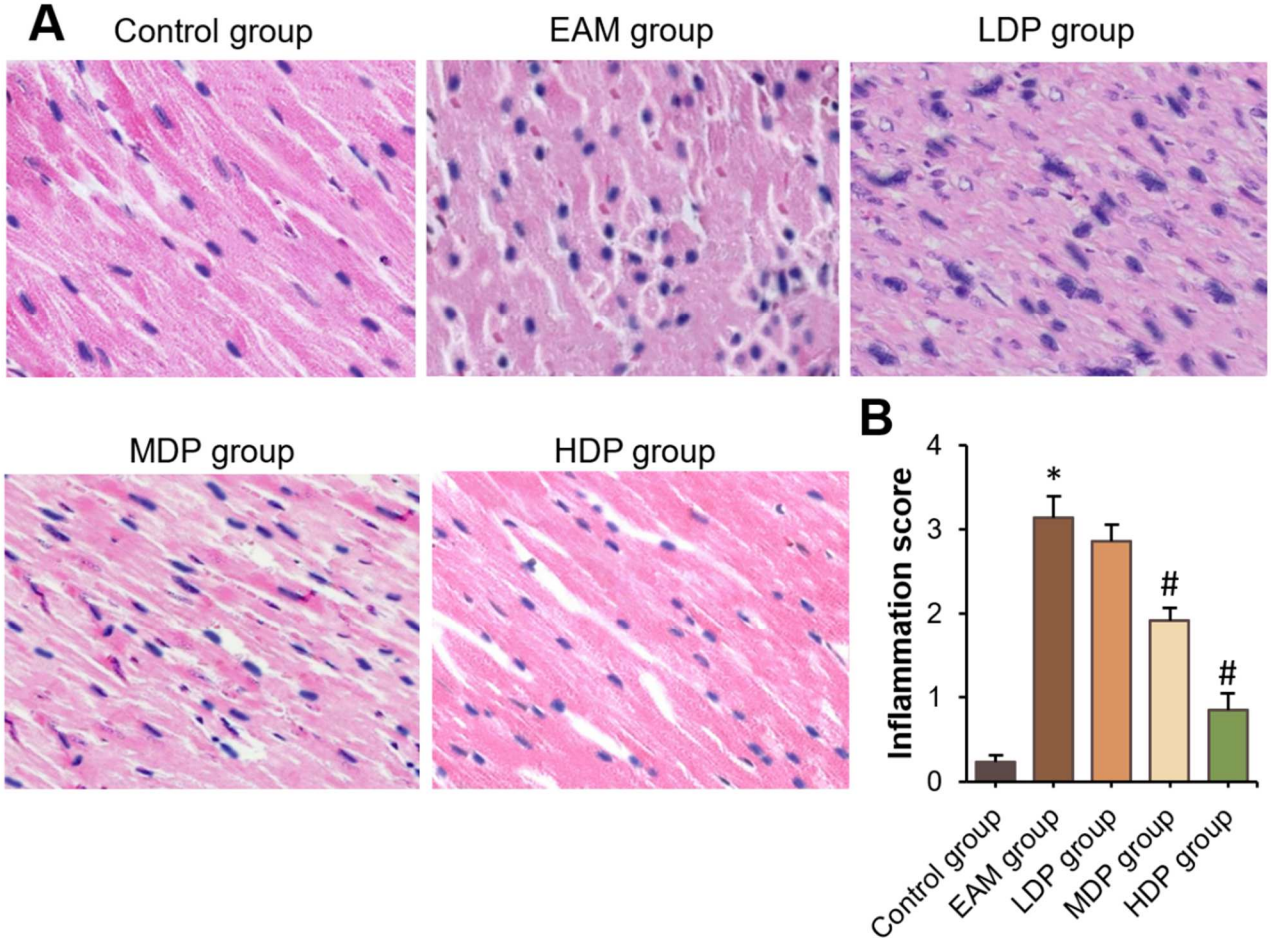

Figure 2. Myocardial morphology observation and comparison among groups. (A) HE staining of myocardial tissue (200×); (B) Myocardial inflammation score.

Contrast of serum cytokine levels among groups: The differences in serum cytokine levels among the different groups of rats were evaluated (Figure 3). The results indicated that serum TNF-α, IFN-γ, TGF-β1, and IL-17 were significantly higher in EAM group compared with the Control group, while IL-4 and IL-10 were considerably lower in EAM group ($P \leq 0.05$). Negligible differences existed in serum cytokine levels between LDP and EAM groups ($P > 0.05$). In contrast, serum TNF-α, IFN-γ, TGF-β1, and IL-17 in MDP and HDP groups were significantly lower to those in LDP group, while IL-4 and IL-10 were significantly higher in MDP and HDP groups compared with the Control group ($P \leq 0.05$).

Contrast of myocardial inflammatory gene expression among groups: The differences in myocardial inflammation-related gene expression levels, including MMP-3, MMP-9, TIMP-1, IL-1β, and iNOS, were evaluated among different groups (Figure 4). Relative levels of MMP-3, MMP-9, IL-1β, and iNOS of EAM group significantly surpassed those in Control group, while TIMP-1 relative level was considerably lower in EAM group compared with the Control group ($P \leq 0.05$). Negligible differences existed between LDP and EAM groups in the levels of MMP-3, MMP-9, TIMP-1, IL-1β, and iNOS ($P > 0.05$). MDP and HDP groups showed similar patterns compared to the LDP group. The relative levels of MMP-3, MMP-9, IL-1β, and iNOS were significantly inferior to MDP and HDP groups than in the LDP group, while the relative level of TIMP-1 was significantly higher ($P \leq 0.05$).

Contrast of HMGB1-RAGE pathway protein expression among different groups: HMGB1 and RAGE protein levels of rats were assessed (Figure 5). HMGB1 and RAGE relative protein levels of EAM group significantly surpassed those in Control group ($P \leq 0.05$). Negligible differences existed between LDP and EAM groups in the relative levels of HMGB1 and RAGE proteins ($P > 0.05$). In contrast, HMGB1 and RAGE relative protein levels in the myocardial tissue of MDP and HDP groups were notably inferior to those in LDP group ($P \leq 0.05$).

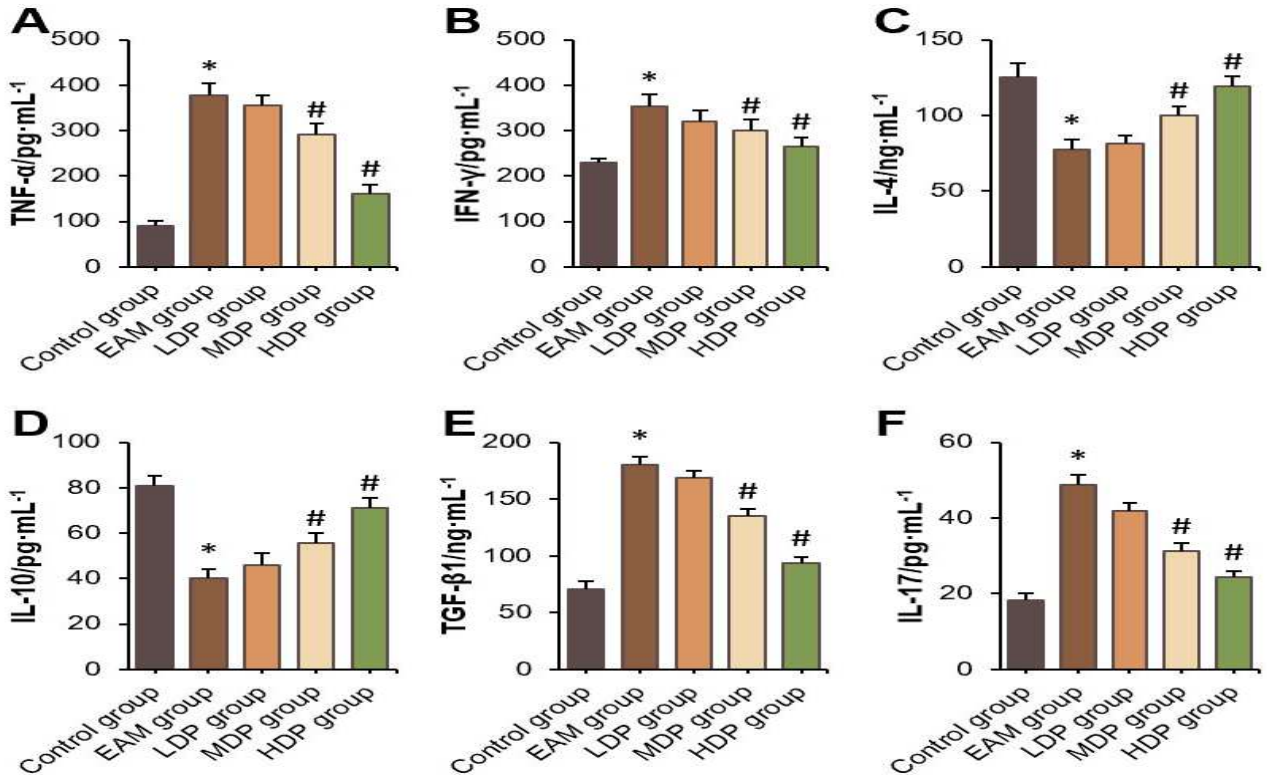

Figure 3. Contrast of serum cytokine levels among groups.

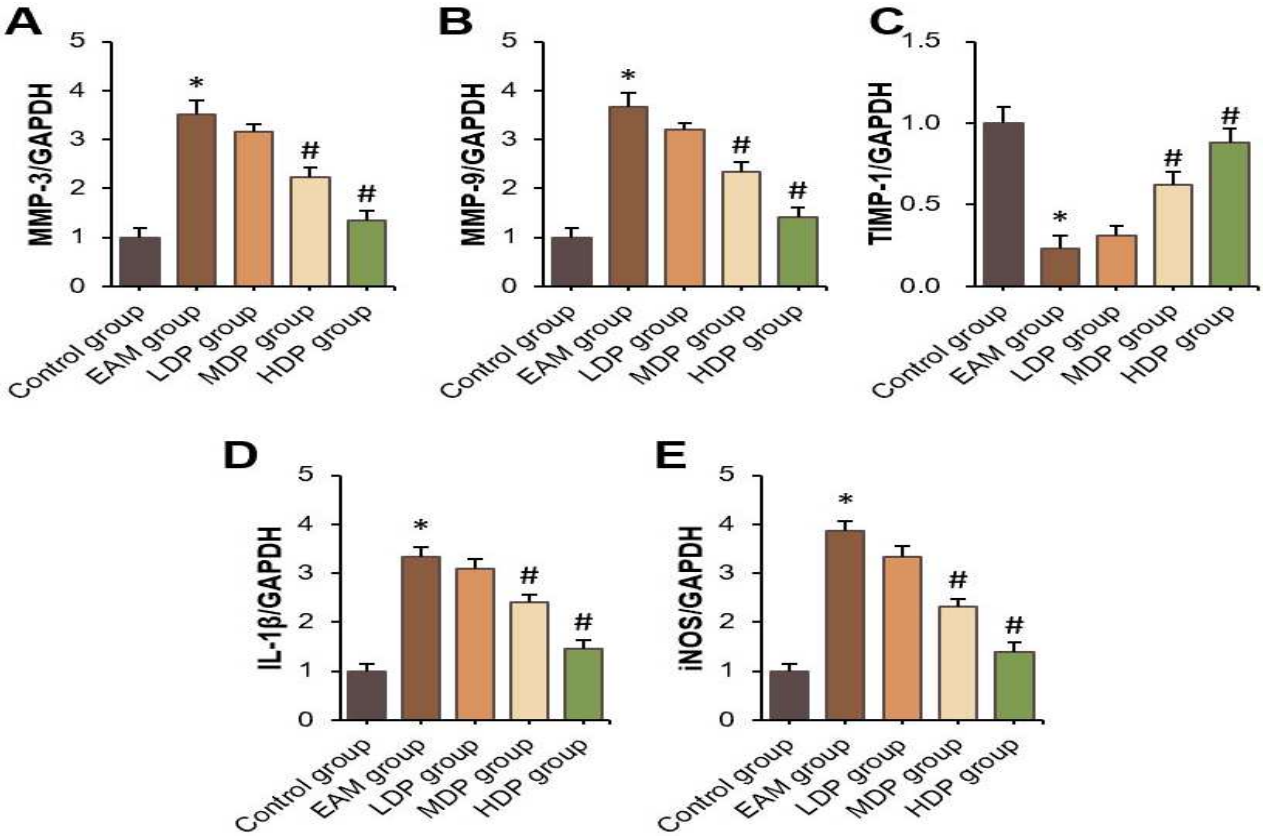

Figure 4. Contrast of inflammatory gene level among various groups of rats.

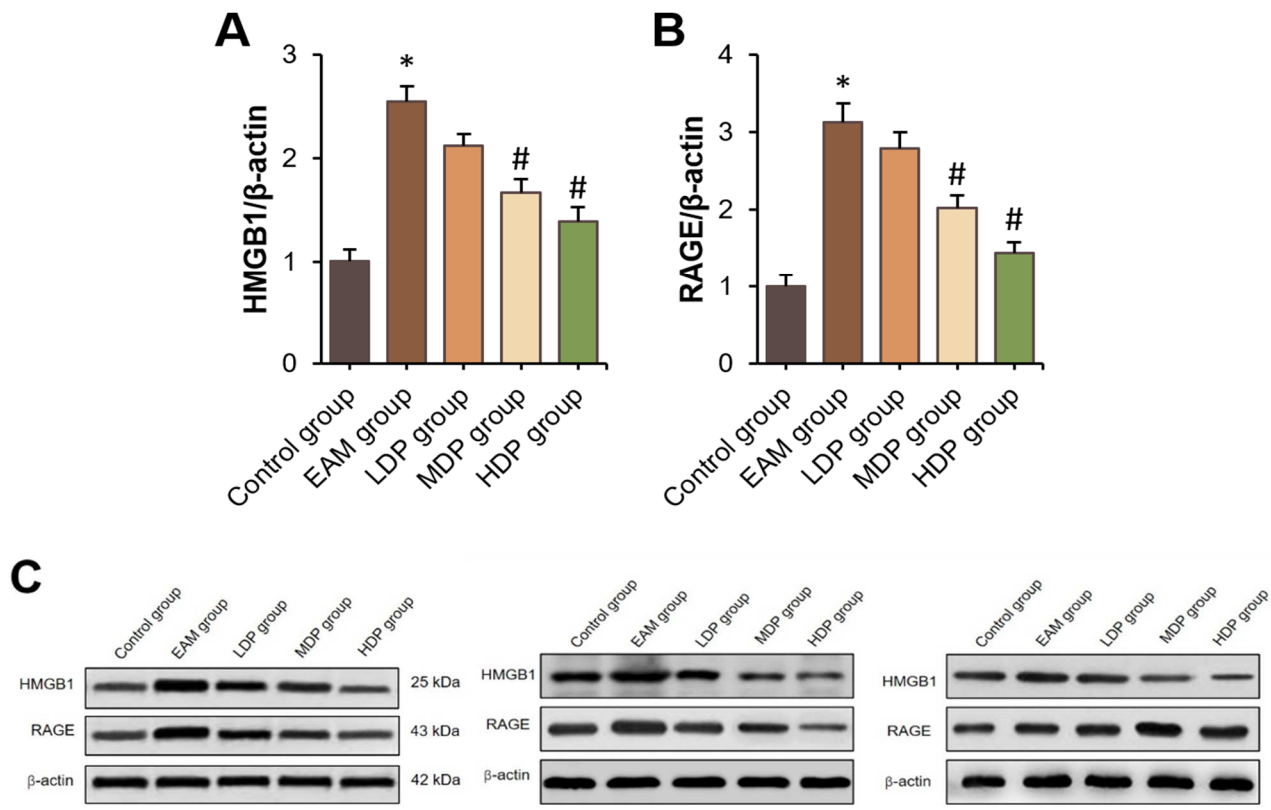

Figure 5. Contrast of HMGB1-RAGE pathway protein levels in myocardial tissue among various groups of rats. (A) HMGB1; (B) RAGE. (C) The Western blot images after three repetitions.

DISCUSSION

The porcine myocardial immunoglobulin injection method was utilized to establish an EAM rat model, and it was found that the LVESD and LVEDD values in the EAM rats were significantly increased, while the LVFS and LVEF values were notably decreased, and the myocardial inflammatory pathology score was also significantly elevated. This suggests that there are significant structural and functional changes in the heart of EAM rats. Furthermore, this study found that after administration of medium-and high-dose propofol, the LVESD and LVEDD values in the EAM rats were significantly reduced, while LVFS and LVEF values were significantly increased, and the myocardial inflammatory pathology score was significantly decreased. This indicates that propofol can improve the cardiac function of EAM rats and alleviate myocardial inflammation damage. The pathogenesis of EAM is still unclear. However, during the development of EAM, it can lead to myocardial cell death and fibrosis. In severe cases, this may progress to dilated cardiomyopathy and cause cardiac functional impairment (Frustaci *et al.,* 2021; Farjoud Kouhanjani *et al.,* 2024; Li *et al.,* 2022).

EAM occurrence is related to changes in T cell subsets. In recent years, cytokines secreted by CD4+ T lymphocyte subsets have been differentiate into Th1 and Th2 cells. Th1 cells primarily secrete pro-inflammatory cytokines, and enhance the cellular immune response (Hohman *et al.,* 2021). Th2 cells, which secrete anti-inflammatory cytokines, help mediating humoral immune responses (Ruterbusch *et al.,* 2020). A shift from Th2 to Th1 subsets can induce the onset and progression of autoimmune diseases (Shang *et al.,* 2024; Rogozynski and Dixon, 2024). Elevated TNF-α, IFN-γ, TGF-β1, and IL-17 were observed in our study, while IL-4 and IL-10 were reduced. This is due to Th1 cells activating macrophages and cytotoxic T cells by secreting TNF-α and IFN-γ, causing myocardial injury (Yu *et al.,* 2023). High expression of Th17 cell cytokines can promote their differentiation and lead to Th17/Treg imbalance, exacerbating inflammatory response (He *et al.,* 2020). This study found that after propofol oral administration, TNF-α, IFN-γ, TGF-β1, and IL-17 in peripheral blood of EAM rats were reduced, while IL-4 and IL-10 were increased. Propofol could regulate the Th1/Th2 imbalance and maintain the balanced immune function (Yu *et al.*, 2022). Similarly, Yu *et al*. found that propofol anesthesia exhibited a lower inhibitory effect on T lymphocytes compared with the sevoflurane and maintained immune function balance by preserving the Th1/Th2 ratio (Yu *et al.,* 2022). Cui *et al*. found that propofol maintained Th17/Treg cell balance and exerted

inhibitory effects on lung cancer cell migration through the γ-aminobutyric acid A receptor (Cui *et al.,* 2022). Another study confirmed that propofol injection reduced the extent of brain damage and maintained Th17/Treg cell balance by modulating IL-17 activity (Cui *et al.,* 2021). In short, propofol can positively regulate the immune function and promote the restoration of Th1/Th2 shift and Th17/Treg imbalance, alleviating myocardial inflammation after EAM.

Our results showed that IL-1β and iNOS in myocardium of EAM rats were elevated, which echoes the findings of Tsuruoka *et al*. (Tsuruoka *et al.,* 2020), indicating the presence of a marked inflammatory response in EAM rats. Additionally, after medium/high doses of propofol treatment, IL-1β and iNOS in the myocardium of EAM rats were considerably reduced. Propofol intravenous injection suppressed IL-1β expression in hippocampal tissue of sleep-deprived rats (Liu *et al.,* 2024). Propofol enhanced the survival rate of human umbilical vein endothelial cells reduced by high glucose and inhibited iNOS expression (Shao *et al.,* 2022). In summary, propofol can alleviate myocardial inflammation in EAM by inhibiting inflammatory gene expression. Increased secretion and activity of MMP-3 and MMP-9 can cause myocardial extracellular matrix degradation (Roczkowsky *et al.,* 2022). TIMP-1 maintains the stability of the myocardial extracellular matrix by inhibiting activity of MMP-9 (Nordeng *et al.,* 2022). Our results found increased MMP-3 and MMP-9 but decreased TIMP-1, indicating the occurrence of extracellular matrix degradation in EAM rats, contributing to cardiac dysfunction. As reported, propofol intravenous injection during primary breast cancer resection significantly reduces MMP-3 and MMP-9 levels (Galoș *et al.,* 2020). Furthermore, when directly acting on glioma U87 cells, propofol inhibits Ki-67, MMP-2, and MMP-9 expression (Li *et al.,* 2021). In our study, after gavage administration of medium/high propofol doses, MMP-3 and MMP-9 in EAM rats were reduced, while TIMP-1 was elevated. Hence, propofol can regulate the expression balance between MMP-3, MMP-9, and TIMP-1, thereby maintaining myocardial extracellular matrix stability after EAM.

After cells are subjected to harmful stimuli, HMGB1 is passively released into the extracellular space and signal surrounding cells, activating cellular immune functions (Foglio *et al.,* 2022; He *et al.,* 2023). RAGE activates downstream signaling mediating inflammatory responses (Lin *et al.,* 2022). HMGB1-RAGE pathway can activate fibroblasts to promote collagen synthesis and deposition, causing myocardial fibrosis (Wang *et al.,* 2022). It can also regulate the expression of MMPs and TIMPs, participating in extracellular matrix remodeling (Malaviya *et al.,* 2020). Monocyte/macrophage infiltration, Th17 cell activation, and pro-inflammatory factor generation are key features of EAM, and HMGB1 promotes the development of EAM by facilitating the transformation of macrophages to the M1 type and promoting the proliferation of Th17 cells (Su *et al.,* 2016). In our study, HMGB1 and RAGE protein levels of EAM rats were elevated. However, after propofol treatment, these protein levels were reduced. Zhao *et al*. showed the same results, which demonstrated that propofol could inhibit the release of inflammatory mediators from cardiomyocytes in a concentration-and time-dependent manner induced by lipopolysaccharide (Zhao *et al.,* 2021). In summary, propofol can reduce inflammatory damage in EAM myocardial cells by inhibiting HMGB1-RAGE signaling.

However, this study has several limitations, including the use of a rodent EAM model that may not fully replicate human disease, unexplored mechanisms of propofol's immunomodulatory effects, lack of dose-response optimization and pharmacokinetic data, absence of long-term outcome assessment, exclusive use of male animals, and administration via oral gavage rather than the clinically relevant intravenous route. Additionally, the study did not examine all potentially relevant inflammatory pathways or include comparator drugs, and the sample size may limit subgroup analyses. While these limitations constrain immediate clinical translation, the findings provide a foundation for future research to validate propofol's therapeutic potential in autoimmune myocarditis.

Conclusion: Propofol alleviated the inflammatory response in the myocardial tissue of EAM rats by modulating Th1/Th2 shift and Th17/Treg imbalance, and inhibiting the expression of inflammatory genes. At the same time, propofol can regulate the balance of MMPs and TIMPs expression to suppress ventricular remodeling in EAM rats. In conclusion, propofol exerts its beneficial effects on improving cardiac function in EAM rats by inhibiting HMGB1-RAGE signaling. These findings provide valuable insights into pathogenesis of EAM and provide insights for the development of new therapeutic targets and drugs for EAM treatment.

Authors' Contributions: Jidong Lv: study concept, design, supervision; Jidong Lv, Lulu Zhang and Sijie Liu: methodology, experiments carried out and data analysis. Jidong Lv: first draft, editing, review and revision of manuscript. All authors agree to publish this article.

REFERENCES

Burnett, G.W., A. Taree, L. Martin and E.O. Bryson (2023). Propofol misuse in medical professions: a scoping review. Can J Anaesth. 70:395-405. English. https://doi.org/10.1007/s12630-022-02382-2.

Chang, Q., J. Wu, Y. An, H. Liu and Y. Sun (2022). Propofol suppresses proliferation, migration,

invasion, and tumor growth of liver cancer cells via suppressing cancer susceptibility candidate 9/phosphatase and tensin homolog/AKT serine/threonine kinase/mechanistic target of rapamycin kinase axis. Hum Exp Toxicol. 41:9603271211065972. https://doi.org/10.1177/09603271211065972.

Cui, C., D. Zhang, K. Sun, H. Li, L. Xu, G. Lin, Y. Guo, J. Hu, J. Chen, L. Nong, Y. Cai, D. Yu, W. Yang, P. Wang and Y. Sun (2021). Propofol maintains Th17/Treg cell balance and reduces inflammation in rats with traumatic brain injury via the miR-145-3p/NFATc2/NF-κB axis. Int J Mol Med. 48:135. https://doi.org/10.3892/ijmm.2021.4968.

Cui, C., D. Zhang, K. Sun, Y. Zhu, J. Xu, Y. Kang, G. Zhang, Y. Cai, S. Mao, R. Long, J. Ma, S. Dong and Y. Sun (2022). Propofol maintains Th17/Treg cell balance in elderly patients undergoing lung cancer surgery through GABAA receptor. BMC Immunol. 23:58. https://doi.org/10.1186/s12865-022-00490-8.

Farjoud Kouhanjani, M., S.A. Hosseini, S.M. Mousavi, Z. Noroozi, P. Sadeghi, A. Jokar-Derisi, M.S. Jamshidi Mouselou, M. Ahmadi and A. Attar (2024). Takotsubo Cardiomyopathy and Autoimmune Disorders: A Systematic Scoping Review of Published Cases. Int J Clin Pract. 2024:7259200. https://doi.org/10.1155/2024/7259200.

Foglio, E., L. Pellegrini, M.A. Russo and F. Limana (2022). HMGB1-Mediated Activation of the Inflammatory-Reparative Response Following Myocardial Infarction. Cells. 11(2):216. https://doi.org/10.3390/cells11020216.

Frustaci, A., M. Francone, R. Verardo, R. Scialla, G. Bagnato, M. Alfarano, C. Chimenti, E. Frustaci, L. Sansone and M. Russo (2021). Pemphigus-associated cardiomyopathy: report of autoimmune myocarditis and review of literature. ESC Heart Fail. 8:3690-3695. https://doi.org/10.1002/ehf2.13474.

Gajić, D., S. Despotović, I. Koprivica, Đ. Miljković and T. Saksida (2021). Ethyl Pyruvate Ameliorates Experimental Autoimmune Myocarditis. Biomolecules. 11:1768. https://doi.org/10.3390/biom11121768.

Galoș, E.V., T.F. Tat, R. Popa, C.I. Efrimescu, D. Finnerty, D.J. Buggy, D.C. Ionescu and C.M. Mihu (2020). Neutrophil extracellular trapping and angiogenesis biomarkers after intravenous or inhalation anaesthesia with or without intravenous lidocaine for breast cancer surgery: a prospective, randomised trial. Br J Anaesth. 125(5):712-721. https://doi.org/10.1016/j.bja.2020.05.003.

He, D.W., D.Z. Liu, X.Z. Luo, C.B. Chen, C.H. Lu, N. Na and F. Huang (2023). HMGB1-RAGE axis contributes to myocardial ischemia/reperfusion injury via regulation of cardiomyocyte autophagy and apoptosis in diabetic mice. Biol Chem. 405:167-176. https://doi.org/10.1515/hsz-2023-0134.

He, X., B. Liang and N. Gu (2020). Th17/Treg Imbalance and Atherosclerosis. Dis Markers. 2020:8821029. https://doi.org/10.1155/2020/8821029.

Hohman, L.S., Z. Mou, M.B. Carneiro, G. Ferland, R.M. Kratofil, P. Kubes, J.E. Uzonna and N.C. Peters (2021). Protective CD4+ Th1 cell-mediated immunity is reliant upon execution of effector function prior to the establishment of the pathogen niche. PLoS Pathog. 7:e1009944. https://doi.org/10.1371/journal.ppat.1009944.

Huang, L., L. Ding, S. Yu, X. Huang and Q. Ren (2022). Propofol postconditioning alleviates diabetic myocardial ischemia-reperfusion injury via the miR-200c-3p/AdipoR2/STAT3 signaling pathway. Mol Med Rep. 25:137. https://doi.org/10.3892/mmr.2022.12653.

Li, F., H. Zhang, F. Wang and Y. Zheng (2021). Mechanisms for propofol in inhibiting the proliferation and invasion of glioma U87 cells and its effect on miR-134 expression. Zhong Nan Da Xue Xue Bao Yi Xue Ban. 46:18-24. https://doi.org/10.11817/j.issn.1672-7347.2021.190734.

Li, X., J. Sundquist, V. Nymberg and K. Sundquist (2022). Association of autoimmune diseases with cardiomyopathy: a nationwide follow-up study from Sweden. Eur Heart J Qual Care Clin Outcomes. 8:79-85. https://doi.org/10.1093/ehjqcco/qcab044.

Lin, L., J. Li, Q. Song, W. Cheng and P. Chen (2022). The role of HMGB1/RAGE/TLR4 signaling pathways in cigarette smoke-induced inflammation in chronic obstructive pulmonary disease. Immun Inflamm Dis. 10:e711. https://doi.org/10.1002/iid3.711.

Liu, H., C. Yang, X. Wang, B. Yu, Y. Han, X. Wang, Z. Wang, M. Zhang and H. Wang (2024). Propofol improves sleep deprivation-induced sleep structural and cognitive deficits via upregulating the BMAL1 expression and suppressing microglial M1 polarization. CNS Neurosci Ther. 30:e14798. https://doi.org/10.1111/cns.14798.

Malaviya, R., E.V. Abramova, R.C. Rancourt, V.R. Sunil, M. Napierala, D. Weinstock, C.R. Croutch, J. Roseman, R. Tuttle, E. Peters, R.P. Casillas, J.D. Laskin and D.L. Laskin (2020). Progressive Lung Injury, Inflammation, and Fibrosis in Rats Following Inhalation of Sulfur Mustard. Toxicol

Sci. 178:358-374. https://doi.org/10.1093/toxsci/kfaa150.

Nordeng, J., H. Schandiz, S. Solheim, S. Åkra, P. Hoffman, B. Roald, B. Bendz, H. Arnesen, R. Helseth and I. Seljeflot (2022). TIMP-1 expression in coronary thrombi associate with myocardial injury in ST-elevation myocardial infarction patients. Coron Artery Dis. 33:446-455. https://doi.org/10.1097/ MCA. 0000000000001128.

Roczkowsky, A., B.Y.H. Chan, T.Y.T. Lee, Z. Mahmud, B. Hartley, O. Julien, G. Armanious, H.S. Young and R. Schulz (2022). Myocardial MMP-2 contributes to SERCA2a proteolysis during cardiac ischaemia-reperfusion injury. Cardiovasc Res. 116:1021-1031. https://doi.org/ 10.1093/ cvr/cvz207.

Rogozynski, N.P. and B. Dixon (2024). The Th1/Th2 paradigm: A misrepresentation of helper T cell plasticity. Immunol Lett. 268:106870. https://doi.org/10.1016/j.imlet.2024.106870.

Ruterbusch, M., K.B. Pruner, L. Shehata and M. Pepper (2020). In Vivo CD4+ T Cell Differentiation and Function: Revisiting the Th1/Th2 Paradigm. Annu Rev Immunol. 38:705-725. https://doi.org/10.1146/annurev-immunol-103019-085803.

Shang, Q., X. Yu, Q. Sun, H. Li, C. Sun and L. Liu (2024). Polysaccharides regulate Th1/Th2 balance: A new strategy for tumor immunotherapy. Biomed Pharmacother. 170:115976. https://doi.org/10.1016/j.biopha.2023.115976.

Shao, J., J. Ding, L. Lu, W. Hou, F. Wang, Z. Sun, H. Jiang and Y. Zhao (2022). Propofol protects against high glucose-mediated endothelial injury via inhibition of COX2 and iNOS expressions. Acta Biochim Biophys Sin (Shanghai). 54:548-555. https://doi.org/10.3724/abbs.2022020.

Su, Z., P. Zhang, Y. Yu, H. Lu, Y. Liu, P. Ni, X. Su, D. Wang, Y. Liu, J. Wang, H. Shen, W. Xu and H. Xu (2016). HMGB1 Facilitated Macrophage Reprogramming towards a Proinflammatory M1-like Phenotype in Experimental Autoimmune Myocarditis Development. Sci Rep. 6:21884. https://doi.org/10.1038/srep21884.

Sun, P., H. Huang, J.C. Ma, B. Feng, Y. Zhang, G. Qin, W. Zeng and Z.K. Cui (2024). Repurposing propofol for breast cancer therapy through promoting apoptosis and arresting cell cycle. Oncol Rep. 52:155. https://doi.org/10.3892/or.2024.8814.

Tschöpe, C., E. Ammirati, B. Bozkurt, A.L.P. Caforio, L.T. Cooper, S.B. Felix, J.M. Hare, B. Heidecker, S. Heymans, N. Hübner, S. Kelle, K. Klingel, H. Maatz, A.S. Parwani, F. Spillmann, R.C. Starling, H. Tsutsui, P. Seferovic and S. Van Linthout (2021). Myocarditis and inflammatory cardiomyopathy: current evidence and future directions. Nat Rev Cardiol. 18:169-193. https://doi.org/10.1038/s41569-020-00435-x.

Tsuruoka, K., S. Wakabayashi, H. Morihara, N. Matsunaga, Y. Fujisaka, I. Goto, A. Imagawa and M. Asahi (2020). Exacerbation of autoimmune myocarditis by an immune checkpoint inhibitor is dependent on its time of administration in mice. Int J Cardiol. 313:67-75. https://doi.org/10.1016/j.ijcard.2020.04.033.

Wang, M., W. Pan, Y. Xu, J. Zhang, J. Wan and H. Jiang (2022). Microglia-Mediated Neuroinflammation: A Potential Target for the Treatment of Cardiovascular Diseases. J Inflamm Res. 15:3083-3094. https://doi.org/10.2147/ JIR. S350109.

Wu, M.B., B. Ma, T.X. Zhang, K. Zhao, S.M. Cui and S.C. He (2020). Propofol improves intestinal ischemia-reperfusion injury in rats through NF-κB pathway. Eur Rev Med Pharmacol Sci. 24:6463-6469. https://doi.org/10.26355/eurrev_202006_21545.

Xie, L., M. Zhao, L. Zong and Y. Yue (2024). Propofol Ameliorates Sepsis-Induced Myocardial Dysfunction via Anti-Apoptotic, Anti-Oxidative Properties, and mTOR Signaling. Discov Med. 36:2088-2097. https://doi.org/10.24976/Discov.Med.202436189.193.

Yamamoto, W., T. Hamada, J. Suzuki, Y. Matsuoka, M. Omori-Miyake, M. Kuwahara, A. Matsumoto, S. Nomura, A. Konishi, T. Yorozuya and M. Yamashita (2024). Suppressive effect of the anesthetic propofol on the T cell function and T cell-dependent immune responses. Sci Rep. 14:19337. https://doi.org/10.1038/s41598-024-69987-z.

Yu, H., L., Chen, C.J. Yue, H. Xu, J. Cheng, E.M. Cornett, A.D. Kaye, I. Urits, O. Viswanath and H. Liu (2022). Effects of propofol and sevoflurane on T-cell immune function and Th cell differentiation in children with SMPP undergoing fibreoptic bronchoscopy. Ann Med. 54(1):2574-2580. https://doi.org/10.1080/07853890.2022.2121416.

Yu, H., L. Chen, C.J. Yue, H. Xu, J. Cheng, E.M. Cornett, A.D. Kaye, I. Urits, O. Viswanath and H. Liu (2022). Effects of propofol and sevoflurane on T-cell immune function and Th cell differentiation in children with SMPP undergoing fibreoptic bronchoscopy. Ann Med. 54:2574-2580. https://doi.org/10.1080/07853890. 2022.2121416.

Yu, M., W. Tang, W. Liang, B. Xie, R. Gao, P. Ding, X. Gu, M. Wang, S. Wen and P. Sun (2023). PCSK9 inhibition ameliorates experimental autoimmune myocarditis by reducing Th17 cell differentiation through LDLR/STAT-3/ROR-γt pathway. Int Immunopharmacol. 124:110962. https://doi.org/10.1016/j.intimp.2023.110962.

Zhang, X., C. Wang, H. Xu, S. Cai, K. Liu, S. Li, L. Chen, S. Shen, X. Gu, J. Tang, Z. Xia, Z. Hu, X. Ma and L. Zhang (2023). Propofol inhibits myocardial injury induced by microvesicles derived from hypoxia-reoxygenated endothelial cells via lncCCT4-2/CCT4 signaling. Biol Res. 56:20. https://doi.org/ 10.1186/s40659-023-00428-3.

Zhang, X., X. Wang, X. Liu, W. Luo, H. Zhao, Y. Yin and K. Xu (2022). Myocardial protection of propofol on apoptosis induced by anthracycline by PI3K/AKT/Bcl-2 pathway in rats. Ann Transl Med. 10:555. https://doi.org/10.21037/atm-22-1549.

Zhao, H., Y. Gu and H. Chen (2021). Propofol ameliorates endotoxin-induced myocardial cell injury by inhibiting inflammation and apoptosis via the PPARγ/HMGB1/NLRP3 axis. Mol Med Rep. 23:176. https://doi.org/ 10.3892/mmr.2020.11815.